Chapter 6

The CERN Antiproton Programme: Imagination and Audacity Rewarded

Vinod Chohan and Pierre Darriulat

6.1 Introduction

The accelerator developments

As early as 1966, C. Rubbia, the Physics Nobel laureate in 1984, had realized the potential of the projected "300 GeV Machine" later built at CERN as the Super Proton Synchrotron (SPS) and proposed to use it as a proton–antiproton collider [1]. Two years later, in 1968, Simon van der Meer, also Physics Nobel laureate in 1984, invented a method to increase the collision rate ("luminosity") [Box 6.1] of the ISR. This was the concept of stochastic cooling [Box 6.2], a brilliant idea. It was published only in 1972 [2], and later proven experimentally at the ISR [3]. This was the necessary ingredient for the bold and imaginative proposal in 1976 [4] of using the CERN SPS as a single ring p–$\bar{\text{p}}$ collider aimed at the discovery of the putative W and Z bosons [Box 6.4].

In 1976 CERN decided to launch two actions in parallel. One was to construct rapidly a small ring, (Initial Cooling Experiment — ICE) to study beam cooling; the other was to set up a design group for a p–$\bar{\text{p}}$ facility using the SPS as a storage ring and collider. Meanwhile, many experimental tests in the ISR, further theoretical developments, and most importantly, the successful test of a faster and more efficient method of longitudinal cooling in ICE confirming cooling in all planes [5], gave the confidence that with stochastic cooling and stacking an overall increase in antiproton density from the production target to the final accumulated beam core of over 10^9 particles could be achieved. Although the cooling times obtained (10 s) were still about 30 times longer than required, it was decided to go ahead with the construction of the Antiproton Accumulator (AA) based on stochastic cooling. The AA was the key element of the scheme, a fixed magnetic field, single storage ring, designed to accumulate antiprotons at 3.5 GeV/c, generated from 26 GeV (PS) protons impinging on a metal target.

The stochastic accumulation (stacking) process, an essential feature in the AA scheme, could not be tested in ICE. This process involved simultaneous cooling in both transverse planes and increasing the longitudinal density by four orders of magnitude while moving the particles into the dense core. This was the biggest gamble in the launch of the AA because it could only be studied in detail by theoretical calculation. Fortunately, in this respect the AA performed as expected.

The AA project was launched in 1978, with beam commissioning in July 1980. The first SPS proton–antiproton collisions at 270 GeV occurred in July 1981 and the first real period of physics runs in 1982. After the W and Z discovery, Nobel awards in 1984 and the ever-increasing appetite for higher luminosities, the Antiproton Collector (AC) ring was built and commissioned in 1987, to bring a ten-fold increase in the accumulated antiprotons. The SPS ran as a collider as well as for short fixed-target runs during these years. After the last collider run in 1991 [6], the SPS returned to its mode as a fixed-target physics accelerator.

The systems and processes described here briefly represent major technological innovations and breakthroughs for the antiproton programme at CERN; similar, improved systems were adapted later for the antiproton source at FNAL/USA, leading to the top quark discovery there in the 1990s.

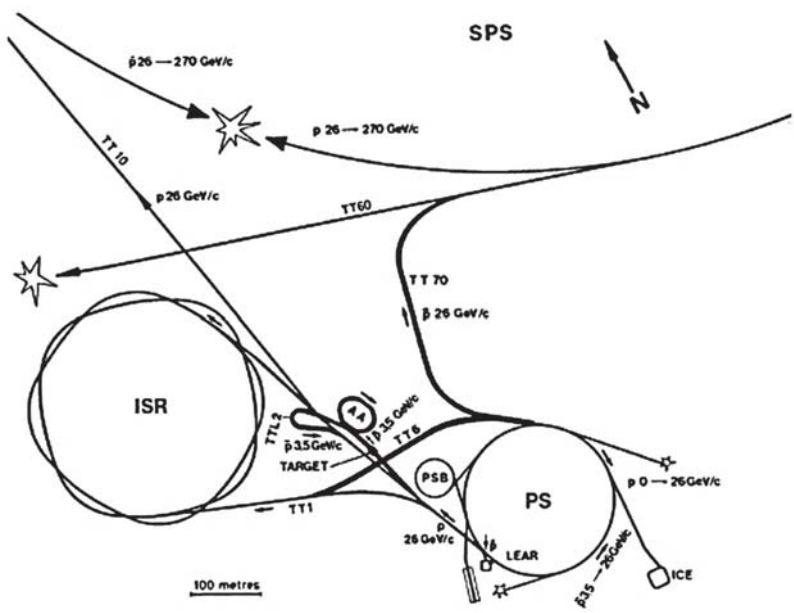

Fig. 6.1. The layout of the CERN accelerators in 1981 with the existing and new tunnels (thick lines) constructed for beam transfer from the AA to the PS, ISR & SPS [1].

Luminosity **Box 6.1**

Luminosity, L, is a figure of merit of the instantaneous rate of events at a particular interaction point of a collider [Box 4.1]. For a given process having cross-section σ_i, the event rate is $\sigma_i \cdot L$. The cross-section is measured in barns, where 1 b = 10^{-24} cm^2. Event rate is measured in Hz, so luminosity is measured in cm^{-2} s^{-1} (or b^{-1} s^{-1}). Except in the special case of continuous beams (ISR), luminosity is proportional to the number of particles per bunch N_b squared and the local rate of bunch encounters, and it is inversely proportional to the transverse area of the beam at the interaction point $s_x \cdot s_y$ where s_x and s_y are local horizontal and vertical beam sizes. Thus, N_b and the bunch encounter rate have to be maximized while $s_x \cdot s_y$ has to be a minimum (i.e. the beams have to be strongly focused). *In a circular collider*, the rate of bunch encounters is given by the product of the number of bunches k_b circulating and the revolution frequency. N_b *is limited* by the performance of the injector, by instabilities arising from bunch-vacuum tube interaction, and by effects between the opposite beams in the interaction points (beam–beam effect). To limit adverse beam–beam effects the beams are separated at crossing points without an experiment. The *total beam current* $k_b \cdot N_b$ is constrained — in e^+e^- colliders by the available RF power replacing the energy lost by the beam due to synchrotron radiation or by cryogenic power required to cool the superconducting RF cavities; in p–p colliders, by particle losses tolerated by the superconducting magnets; in p–$\bar{p}$ colliders, by the performance of the $\bar{p}$ injector. The *beam sizes* s_x, s_y to be minimized are determined by the square root of the product $\beta_i \cdot \varepsilon_i$ where β_i is a local magnet lattice parameter, inversely proportional to the focusing strength, and ε_i, is the beam emittance, i.e. the area of transverse phase space occupied by the beam. Small β requires strong local focusing: this is produced by a sequence of quadrupoles on either side of the interaction point forming a so-called *low-β insertion*. In e^+e^- colliders, synchrotron radiation effects lead to an equilibrium value of ε_i that grows with the square of beam energy. In hadron colliders, the injector determines the invariant $\beta_b \cdot \gamma_b \cdot \varepsilon_i$ where β_b and γ_b are the relativistic parameters of the beam, so ε_i shrinks during acceleration — an advantage for high energy colliders. The beam intensity and the beam size also vary with time: the beam intensity decreases due to collisions with residual gas and with the opposing beam. While the beam sizes are nearly constant in e^+e^- colliders, in hadron colliders they increase for the same reasons as beam loss occurs. For the experiments, the relevant parameter is L *integrated over time* and is measured in terms of barn^{-1}. It is optimized by a careful programming of the operation cycle of injection, beam acceleration, luminosity production, and beam dump. In a *linear e^+e^- collider*, the rate of bunch encounters is given by the number of bunches in the bunch train times the repetition frequency. The latter is only about 100 Hz, so high-intensity bunches are imperative, and these must be very tightly focused at the interaction point. This adds to the focusing but also creates synchrotron radiation — which causes a spread in centre-of-mass energy and background in the detector. Longitudinally polarized beams were achieved at the SLC and are planned for future linear e^+e^- colliders. This feature which enhances the effective luminosity and enables improved discrimination between weak-interaction processes by choice of spin directions [Box 2.2] of the interacting particles.

Supplying antiprotons to the SPS as a collider

The overall scheme (Fig. 6.1) involved some major modifications to the PS and the SPS and the construction of new beam transfer lines for the antiprotons. The scheme evolved over the years improving continuously the performance.

The PS injectors, the 50 MeV Linac, the 800 MeV booster-synchrotron and the 26 GeV PS were pushed to their limits to deliver an intense proton beam on the production target with an intensity of up to 1.4×10^{13} protons per pulse, as much as the target could withstand, yielding up to 7×10^7 injected antiprotons. The transverse emittances had to be small to permit focusing to a small size over the whole length of the target. Finally, the proton burst length had to correspond to the AA circumference, exactly one quarter of the PS.

Initially, the AA was used as a collector as well as an accumulator; in 1987 the ACOL project was launched with the construction of a large acceptance Antiproton Collector (AC) ring encircling the AA, for collecting the antiprotons from the target; this permitted a 10-fold increase in the accumulated particles. A powerful RF system (1.5 MV, 9.5 MHz) in the AC reduced the momentum spread by a factor four before cooling was applied. Stochastic cooling in the AC reduced the six-dimensional phase space density by up to 4×10^9 before the beam was bunched by an RF system and extracted to the AA, where the beam was accumulated over hours or days.

In the AA, complementary stochastic cooling systems acted continuously on the antiproton stack. Over a day, a stack with a dense core of several 10^{11} antiprotons was accumulated. An antiproton bunch was picked from the stack and moved to the ejection orbit. From there it was sent through a "loop" (TTL2, Fig. 6.1) to the PS. In the PS, this bunch was accelerated to 26 GeV/c and sent to the SPS.

Prior to a transfer, checks were performed, concluded by the dispatch of a small "pilot bunch" of $\sim 10^9$ antiprotons all the way from the AA to the SPS. This assured that the big shots (up to 6 bunches), containing a day's worth of accumulated antiprotons, would safely find its way. The antiproton beam was accelerated in the SPS to the top energy of 270 GeV simultaneously with the counter-rotating proton beam which had been injected just before the antiproton transfer. After some adjustments the beams were brought into collision. The acceleration time of ~ 3.4 s was short compared to the time the beams were kept colliding with typically up to 16 h of useful beam lifetime.

The AA and AC storage rings

The AA had a circumference of 157 m. Its magnetic field was constant, for a beam momentum of 3.5 GeV/c on the central orbit. It was installed in a new hall

and covered with concrete shielding blocks. Figure 6.2 (left) shows the AA and the AC rings, before being covered with concrete shielding. Figure 6.2 (right) shows the layout of the two rings with the "dog-leg" incorporated in the antiproton injection line to diminish the flux of secondary electrons and pions reaching the hall.

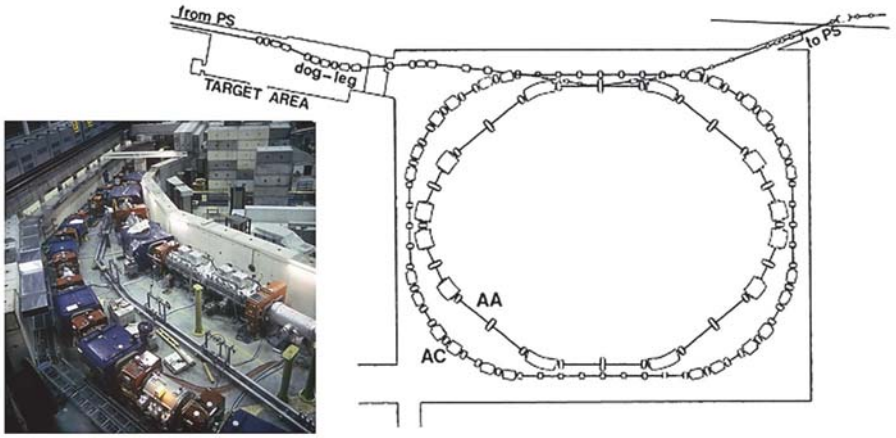

Fig. 6.2. The AC ring built around the AA ring, and a partial view of the installation.

The circumference of the AC was 187 m. It was installed around the AA in a period of just eleven months in 1986–87. Its primary task was to capture an order of magnitude more antiprotons than the AA, for which it had much larger acceptances, both, in transverse and in momentum space.

The AA, and later the AC had to have a large acceptance in order to capture a maximum number of antiprotons coming from the target. The phase volume occupied by the beam had therefore to be reduced and the particle density in phase space increased. In fact, the density in 6-dimensional phase space (the particles have position and momentum in transverse and longitudinal directions) had to be boosted by nearly a factor 10^9 in the AA. The only way to achieve this was to fully exploit the method of stochastic cooling.

To this end, the AA was the first accelerator in the world to be equipped with a full set of stochastic cooling systems; there were 7 systems (frequency range 150 MHz to 2 GHz): a precooling system for the momentum plane and 3 systems, one for each phase plane for stack-tail and core regions [7]. With the arrival of the AC ring, the AA systems were converted to 5 systems, operating in the higher frequency range of 1–8 GHz [8]. The AC had 9 systems in 3 bands (1–3 GHz) applying cooling in all three phase planes in each band [8]. All these systems had their specific functionalities and significant variations in pickup-kicker

technology, amplifiers, gains, bandwidths and optimization. For example, in the AC, both pickup and kicker transverse apertures followed a programmable mechanical movement in time to keep in step with the transverse beam dimensions as the cooling progressed during the 4.8 sec that the beam stayed in the AC before ejection towards the AA. The components at low RF power (pickups, terminations, preamplifiers) were cryogenically cooled (20 K at the terminating resistors) to reduce thermal noise. Common amplifiers were used to switch from transverse to longitudinal plane systems at appropriate times in the AC cycle.

Overall, the AC & AA stochastic cooling systems constituted as high-power, low-noise, cryogenic multi-band microwave systems, with multiple transmission lines, feed-throughs and fast-moving electrodes in ultra-high vacuum.

The SPS and its modifications as a proton–antiproton Collider

The SPS started collider operation in 1981 at 270 GeV (centre-of-mass, CM, energy 540 GeV), for the same magnet power dissipation as the 400 GeV accelerator cycle. In 1984, increased water cooling of the magnets allowed the CM energy to be pushed to 630 GeV. For short periods of operation, a pulsed mode, cycling between 100 GeV and 450 GeV, extended the collider reach to 900 GeV CM energy. Usually, there was one "fill" per day, and the beams were dumped when the luminosity had become too low for the experiments to take useful data.

The fixed-target machine SPS had to be significantly modified to function as a collider from 1978 onwards in parallel to the AA construction. The machine needed increased beam focusing at the two collision points. Two huge underground experimental areas were constructed: The UA1 and UA2 detectors had to be retractable to avoid high levels of radiation during the period of the yearly fixed-target physics run. Functioning as a storage ring required a considerable improvement in the vacuum system. The RF system needed many modifications to simultaneously accelerate protons and antiprotons with precise synchronisation between bunches of the counter-rotating beams and to bring them to collision at the two experiments. Earlier studies of using SPS as a collider had indicated that RF noise could be a limiting factor for beam life-time; the various sources of noise in the closed loop RF system were analysed and their influence reduced sufficiently. The SPS had been built for an injection momentum of 14 GeV/c. The injection system had to be modified to permit 26 GeV/c proton injection via the TT10 transfer line, which also had to be upgraded. For the counter-clockwise circulating antiprotons a new transfer line, TT70, had to be built from the PS to the SPS and a new injection system installed for 26 GeV/c antiprotons. With the tenfold increase in antiproton production from 1987 onwards and collisions with

6 bunches in each beam (up to 10^{11} particles/bunch), a peak luminosity of 3×10^{30} cm^{-2} s^{-1} was eventually reached, having increased by a factor of 60 since 1982.[a]

The low energy programme spawned by the p–$\bar{p}$ collider: LEAR and AD

Low-Energy Antiproton Ring (LEAR)

Initially, the scheme [9] was proposed as a 'parasitic' user, using only a small fraction of the accumulated antiprotons in AA, the main client still being the SPS Collider. Antiprotons at 3.5 GeV/c were returned from the AA to the PS for *deceleration* from 3.5 GeV/c to 0.6 GeV/c and transferred to LEAR, where they were further decelerated to below 100 MeV (or accelerated up to about 2 GeV); the antiproton beam was extracted into the PS South Hall for different experiments at dedicated beam lines. One of the major highlights and technical innovation was the development of a technique for ultra-slow extraction; the LEAR beam of modest quantity would remain circulating for many hours and an extremely feeble quantity of antiprotons (equivalent and down to about one antiproton per turn) would be extracted using this special technique [Highlight 6.4].

Antiproton Decelerator (AD)

LEAR operated until end 1996. However, with the approval of the LHC in 1994, the scheme conceived originally for the SPS Collider was considered too expensive to continue providing low-energy antiprotons for the small but vibrant physics community at LEAR. This spawned the idea converting the AC into a multi-function Collector and Decelerator of antiprotons with extraction for physics into the middle of the ring, within the existing Hall. In this scheme, the target area for antiproton production remained unchanged but the AC ring was modified to permit ramping from the injection momentum of 3.5 GeV/c down to 100 MeV/c and an extraction channel for experiments was installed in the AD Hall. In 1997, the AA was dismantled, LEAR closed down and the AC was converted into the AD [9].

While the AD extracted beam energy of 5.3 MeV was adequate, it was still a far cry from the needs of the antiproton trapping experiments which required use of degrader foils to further decelerate, losing however almost 99% of the beam in the process. This led to the innovative idea to use a radio-frequency quadrupole to decelerate the antiprotons even further, down to 10 keV, for a particular physics experiment ASACUSA [Highlight 6.3]; The Extra Low-ENergy Antiproton ring (ELENA) under construction at CERN today envisages AD extraction into this lower stage decelerator from a momentum of 100 MeV/c to 13.7 MeV/c (kinetic energy 100 keV).

[a] The editorial team thanks Lyn Evans for his contribution to this chapter.

The experimental programme

In 1976, when Carlo Rubbia proposed to produce the putative weak bosons in proton-antiproton collisions in the SPS, the prestige that such an important discovery would mean for European physics in general and for CERN in particular convinced the physics community and the CERN management that the risk was worth taking: the short time table and the relatively low cost of the project matched well the window of opportunity open in the pre-LEP period. However, as many in the accelerator community were frightened by the "beam acrobatics" implied by the proposed scheme, and as many in the Fixed Target community were upset to see part of the SPS time slip out of their hands, approval of the project was subjected to three conditions: positive outcome of a feasibility study that was immediately initiated; success of a feasibility test of stochastic cooling (ICE) that was concluded in Summer 1978, providing evidence for fast cooling in both transverse and longitudinal phase space; setting up of a detector study group, under Rubbia's chairmanship, aimed at showing the feasibility of experimentation in general and of detecting the W and Z bosons in particular. The work of this study group served as the basis for the design of the UA1 detector [10].

In June 1978, the SPS committee approved the UA1 experiment and encouraged the submission of a second proposal. UA2 was approved in December 1978. The first proton-antiproton collisions were observed in June 1981. The W and Z bosons were detected soon after, and Carlo Rubbia and Simon van der Meer (Fig. 6.3), thanks to whom the discovery was made, were awarded the 1984 Nobel prize for "their decisive contributions to the large project which led to the discovery of the field particles W and Z, communicators of weak interactions" [10, 11].

Fig. 6.3. Carlo Rubbia and Simon van der Meer following the announcement of the Nobel Prize.

Detectors for the W- and Z-boson discovery

The detection of the weak bosons was less of a challenge than their production. Their large invariant mass made it easy to eliminate promptly, at trigger level, the low transverse momentum particles produced in the vast majority of proton-antiproton collisions: the problem was their identification among the selected sample of high mass, centrally produced final states, dominated by pairs of hadron jets. It was solved by selecting their leptonic decays, namely $W \rightarrow e\nu$ or $\mu\nu$ and $Z \rightarrow ee$ or $\mu\mu$, expected to give a clear signature, in spite of their low branching fractions (20% and 6.5%, respectively). To the extent that the misidentification of a hadron jet faking a lepton could be kept below one part in ten thousand, clear W and Z signals were expected. It was important that the detector could measure the sign of the lepton charge, allowing for an elegant probe of the nature of the weak interaction: in W decays, the positive lepton is preferentially emitted along the antiproton beam, the negative lepton along the proton beam.

Experience with the operation and exploitation of so-called 4π detectors, namely detectors surrounding the beam interaction region as completely as possible, was still embryonic when UA1 and UA2 had to be designed. However, at that time, other detectors were already being conceived for upcoming electron-positron colliders, using the experience of MARK I at SPEAR. In the case of hadron colliders, the constraints on detector design were stronger but one knew pretty well, from experimentation at the ISR, how such detectors must look like. The importance of efficient and accurate calorimetry was well understood, in particular for the detection of the transverse momentum imbalance caused by the presence of a non-interacting neutrino in W decays. Insensitive zones would be very damaging in this respect; detectors had to be, as one said, "hermetic". A major unknown was how "hostile" the collider environment would be, and how much one would have to protect the detectors from the background produced by beam losses. The collider turned out to be remarkably "quiet", producing much less background particles than anyone of us had anticipated, facilitating the experimentation.

The UA1 detector [12] had been designed as a multipurpose detector with no right to fail or to be blind to any significant manifestation of the new physics to be explored. It had to cover as large as possible a solid angle, to detect individual hadrons, hadron jets, electrons as well as muons. Its design precisely met these objectives. This spectrum of detection possibilities, however, had been obtained at the price of compromises on the performance of individual components, in particular the quality of the calorimetry and the strength and configuration of the magnetic field. The technically safe choice of a warm shoe-box-like dipole, rather than a superconducting solenoid, limited the field to 0.7 T and imposed the

presence of dead regions in the field direction and in the gap between the two half-yokes. Moreover, it severely limited the segmentation of the hadron calorimeter, fitted in the magnet yokes, and of the electron calorimeter, lacking azimuthal segmentation. The main strength of the UA1 detector was a large-volume, high-resolution central tracking detector of an original and high-performing design. Its remarkable pioneering achievements make it without any doubt a major technological highlight of particle detection at the proton–antiproton collider [Highlight 6.5].

UA2, the second detector [13], had been approved under the condition of being cheaper than UA1 (by about a factor three, as it turned out) (Fig. 6.4). Moreover, it had to be constructed and assembled in less than three years in order to catch up with UA1. Such constraints imposed restrictions on its design: it would detect electrons but not muons, it would focus on the central rapidity region and would not measure particle charges except in two cones along the beams where the W decay charge asymmetry was expected to be maximal. The central high resolution calorimeter, of a very careful and precise design, was innovative in several of its features, in particular its projective geometry and the use of special thin plastic plates ("wavelength shifters") to collect separately the light from different sections of the lead-scintillator lamination [Box 6.3]. It proved to be a superb tool for the

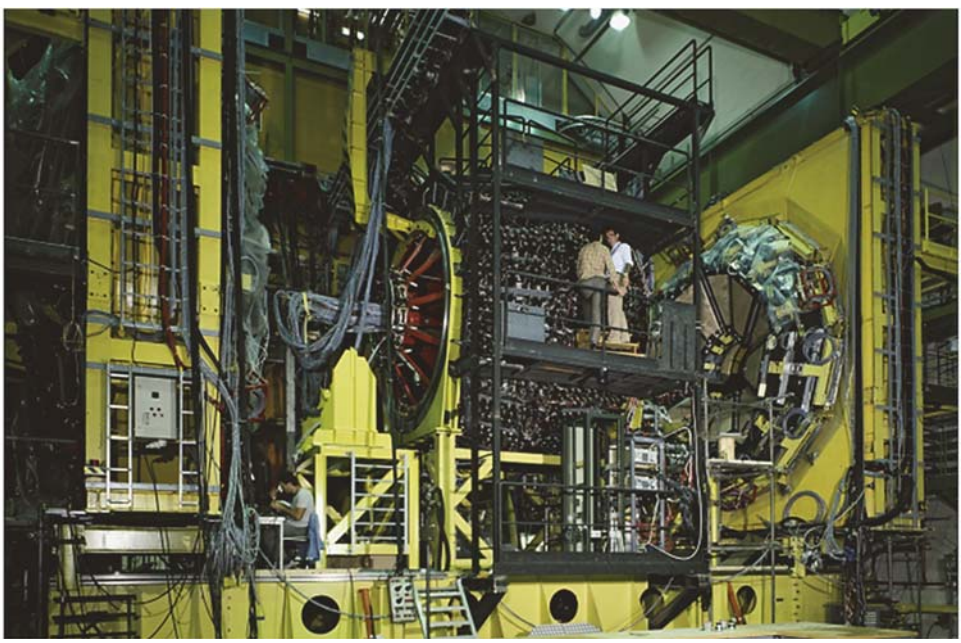

Fig. 6.4. UA2 detector during construction.

detection and energy measurement of electrons and hadron jets. Toroidal magnetic fields in the forward and backward cones did their job in revealing the expected charge asymmetry in W decays but otherwise severely limited the solid angle coverage and the hermeticity of the detector. When the installation of ACOL gave the opportunity to upgrade the detector, they were replaced by calorimeters extending the central structure to smaller angles.

It was also at that time that the central vertex detector, originally a set of cylindrical drift chambers that had to fit in a very small volume around the beam, was replaced by scintillating fibres and silicon pads. While the latter are described in more detail below [Highlight 6.6], the former was the first detector of this type to be used in an experiment; it featured several novel technologies: scintillating fibres as the active detector element, custom image intensifier with integrated CCD readout to collect the signals and custom digitizers to process the images. It included layers of fibre triplets, one parallel and two at opposite small angles relative to the beam, allowing for space reconstruction of the particle tracks and incorporated a layer of lead for initiating electron and photon showers.

The UA1 and UA2 detectors turned out to nicely complement each other. UA1 could do more than UA2: it could detect electrons, muons and tau leptons; observe the branching ratios for the weak bosons decaying into different leptons, a crucial test of the theory; detect muons in the neighbourhood of a hadron jet as a possible signal for new physics, give early evidence that mesons containing a beauty quark could change, "oscillate", between their matter and antimatter forms and make an early and elegant measurement of the W spin. But what UA2 could do, it did better than UA1; it provided the most accurate measurements of the W and Z masses and gave important contributions to the exploration of the strong interaction sector, using its excellent jet detection capability.

The remarkably smooth operation of the CERN proton–antiproton collider has been an opportunity for other experiments than UA1 and UA2 to open new chapters of physics in an unexplored energy domain. The novelty of the experimental environment that it offered and the challenge it presented in terms of experimentation were an incentive to innovate in the design of the detectors.

A particularly successful example is the UA5 experiment [14], which had only a few days to collect its data before the UA2 detector was rolled into the tunnel and yet succeeded in giving to the physics of hadron collisions some very important results. It used two very large streamer chambers, the largest ever used in an experiment, photographed through image intensifiers and triggered by scintillation counters [Box 3.3]. Lead glass converters inside the chamber volume were used to convert photons. Charged particles were detected down to less than a degree, a remarkable achievement.

In the same way as the ISR had been a test bench for the development of detectors used at the proton-antiproton collider, the latter, together with the Fermilab Tevatron, has been a test bench for the development of LHC detectors. Among many such examples, the case of the Roman pots is an interesting illustration. Developed at the ISR to measure the total cross-section [Highlight 4.7], they were revived at the proton-antiproton collider, instrumented with fine resolution detectors which could be placed to the beam within a few millimetres; later they were used to test a silicon strip detector, with six planes totalling 46 000 channels, which became the prototype of an important element of the LHCb detector.

Exploring antimatter

Not to be outdone by the collider detectors, those at LEAR, using nearly stopped antiprotons, displayed much ingenuity in their design. Particularly innovative were two 4π detectors, Crystal Barrel and CPLEAR. The former included a projective assembly of 1380 CsI crystals and a segmented drift chamber operated in a 1.5 T magnetic field; it discovered a new particle considered as the lowest mass scalar glueball. CPLEAR developed a technique to identify the quark (or "flavour") content of the produced neutral kaons, allowing detailed measurements of CP violation [Box 3.4] and placing stringent limits on CPT conservation in weak interactions. The experimental method that was used for identifying the flavour can be considered as a pioneer for some of the methods used today in LHCb.

A major success story of the LEAR experimental programme has been a succession of experiments aiming at precision measurements of the properties of antiparticles, first antiprotons and later anti-hydrogen. The first in the line was the Penning trap experiment, which succeeded in trapping antiprotons and keeping them trapped for up to 2 months. Compared with trapping protons, which had been already done in a few laboratories, the difficulty was to reach a much better vacuum in order to prevent the trapped antiprotons from interacting and annihilating with the normal matter of the residual gas. The experiment verified the equality of the antiproton and proton charge-to-mass ratios with an accuracy of 1 part in 10^{10}. In parallel with these advances in trapping techniques, formation of anti-hydrogen atoms was observed in flight in 1996 for the first time [Highlight 6.7]. This double success paved the way to the trapping of anti-hydrogen that was achieved at LEAR in 2002 [15] by the two successor experiments, ATHENA and ATRAP. Other remarkable contributions of LEAR to atomic physics include studies of antiprotonic helium and the X-ray spectroscopy of protonium, the exotic atom of a proton and an antiproton orbiting each other. These successes were at

the root of the recent decision to continue fundamental research on antimatter at CERN with the addition of the ELENA ring.

Looking back at the early days of the proton–antiproton collider and the many contributions it gave to fundamental particle, nuclear and atomic physics, one cannot help but being impressed by the role it played in technological advances, which lead to the construction and exploitation of the LHC. Progress on the two fronts feed each other, accelerating the rate of innovative achievements in each of them. The degree of sophistication, in both accelerator and detector technology, which prevailed at the collider was inconceivable at ISR time, as that which now prevails at LHC was unconceivable by then. Yet, all this happened in less than fifty years. It is the pride of CERN, together with the Fermilab Tevatron, to have hosted and fostered such progress so successfully.

6.2 Stochastic Cooling: Technology to Compress the Beams

Fritz Caspers and Lars Thorndahl

Stochastic cooling of particle beams, pioneered by CERN, was a condition *sine qua non* for the feasibility and success of the proton–antiproton collider. The required novel technology was developed by a small team, whose nucleus had been formed for the cooling tests at the ISR and included S. van der Meer, the inventor of stochastic cooling. The development concentrated in particular on electrodes, picking up with high selectivity the signal from the beam, the "pick-ups" (PU), and on the pulsed elements (kickers) imparting a kick to the beam particles derived from the signal of the PUs [Box 6.2]. The signal on its way from the pick-up electrode (PU) to the kicker had to be conditioned, without introducing significant delays, such that the signal generated by a beam slice at the PU would arrive in time to impart a corrective kick on the same beam slice (Figure in Box 6.2). Cooling of transverse deviations requires a transverse kick, longitudinal cooling (i.e. in the beam direction), reducing the energy spread and increasing the longitudinal density, requires acceleration or deceleration of the slice. The signal treatment between the PU and kicker needs amplification in well-defined frequency bands and filtering. The systems must have a wide microwave bandwidth as the cooling rate is proportional to the bandwidth of the system. For technical reasons the bandwidth of a system is typically limited to an octave, so the required total bandwidth is often covered with several systems operating in adjacent ranges of frequency. The coupling to the beam should be as strong as possible to keep the power of the amplifier inserted between PU and kickers relatively low [16]. A few prominent examples of these technologies, some of which were at the time at the limit of feasibility, are given below.

Stochastic cooling: Domesticating beams **Box 6.2**

The purpose of stochastic cooling [1, 2] is to increase the density of a beam of charged particles. During this process, the particles are "compressed" into a denser beam with less angular divergence and less energy spread: empty space between the particles is squeezed out. The phase space occupied by the beam is reduced so that a new beam can be added during beam accumulation in the limited phase space of the accelerator, and the final beam can be made denser, imperative for achieving good luminosity in antiproton colliders. Cooling is also used to prevent the blow-up of a stored beam.

The principle of stochastic cooling is illustrated for the case of reducing the wide horizontal dimension of a beam caused by oscillations of the particles around the nominal orbit. Consider first a single particle. A sensor (pick-up) acquires an electrical signal proportional to the displacement of the particle (see Figure) [1]. The signal takes a short-cut across the ring so that the particle receives the kick required to put it on the nominal orbit. Fast signal transmission from pick-up to kicker is vital for the cooling system, as the particles move close to the speed of light. In reality, pick-up and kicker act on a short slice of the beam which contains a small fraction of the total number particles N. The slice/sample duration is determined by the bandwidth W of the electronics. The damping of the oscillation of the particle is disturbed by the signals from the other randomly distributed particles in the slice. Given the finite number of particles and the sample containing different particles at each pass due to a spread in revolution frequencies (perfect mixing), the displacement of the slice will be different at each passage. The effect of the companion particles in the sample averages out to first order but they produce a second order adverse blow-up of the beam depending on the gain of electronic system. For a properly chosen gain the correction of many samples leads to a slow increase in beam density, i.e. cooling, at a rate $\propto W/N$. So high bandwidth is imperative, and the system works well for low N, typical of antiproton beams. Cooling rate is also reduced by imperfect mixing; thermal noise in the electronics, the power limit of the large-band amplifiers, and pick-up to kicker time-of-flight errors. Longitudinal cooling to reduce the energy spread in a beam and increase longitudinal density works according to the same principle. To sense the energy deviation, a pick-up is used at a point on the orbit where an energy error leads to a large transverse displacement. The signal feeds a kicker producing a longitudinal kick. Transverse and longitudinal cooling must be combined to achieve high beam density.

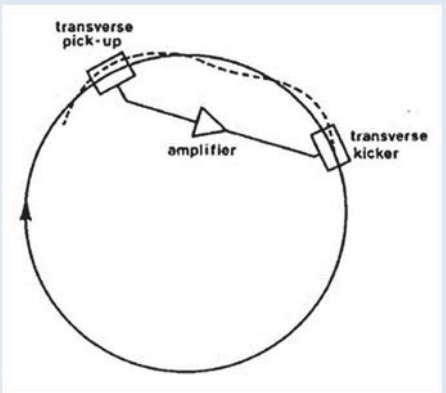

[1] S. van der Meer, *Rev. Mod. Phys*. **57**, 689-697, (1985).
[2] D. Möhl, *Stochastic Cooling of Particle Beams* (Springer-Verlag, Berlin, 2013).

For the cooling of the longitudinal momenta of the beam particles a method based on *filters with periodic frequency behaviour* was invented [17]. Longitudinal cooling must be sensitive to the different longitudinal momenta of the particles, making use of their slightly different revolution frequencies. The spread in longitudinal momentum is reduced by comparing the revolution frequency of the particles to the nominal value and by a subsequent correction of the deviation with an electric kicker field in a downstream gap, either accelerating or decelerating. The comparison is accomplished by a filter between the PU and kicker which generates the appropriate phase-shift of the signal, depending on the deviation detected leading to acceleration or deceleration. Such filters, having extremely high selectivity, were based on transmission lines with a length corresponding to the nominal revolution frequency. The signal of the beam slice is generated by a PU and amplified before filtering, yielding an excellent signal-to-noise ratio after amplification. This advantage is particularly relevant if the beam has a very narrow energy spread.

Novel *slot-type structures* [18] were developed for both PUs and kickers, for frequencies above 1 GHz, a frequency range not covered by the technology available at the time (coupling loops). They were superior to the loops, which are not wide-band and had no means for the suppression of undesired waveguide modes. The same type of structure acts as both PU and kicker for stochastic cooling of both transverse and longitudinal momentum spread. In order to improve the signal-to-noise ratio at the PU many of these elements were used in a sequential array in the ring. This type of structure was first tested and put into use in the ISR and later adopted for the Antiproton Accumulator (AA). Furthermore, these structures have the attractive features of constructional simplicity and requiring only a small number of vacuum feedthroughs. Figure 6.5 shows such a structure with the coupling slots between the beam chamber and pairs of (TEM) transmission lines on top and bottom. In a PU, these lines transmit the signal from the beam to the amplifier, and when used as kicker transmit the signal from the

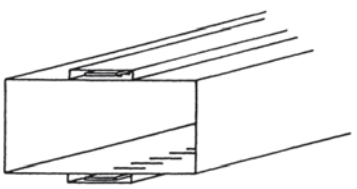

Fig. 6.5. Slot-type PU or kicker. The beam circulates at the centre of the chamber [16].

amplifier to the beam. signals from the individual slots add up to give strong coupling, provided that (i) the slots are small compared to the wavelength of the signals and (ii) the phase velocity in the transmission lines transporting the signal equals the particle velocity which is close to the velocity of light.

In order to satisfy the ever-increasing appetite of antiproton users, the Antiproton Collector (AC) was built around the AA in 1986. From 1987 on, it boosted the accumulation rate, eventually by an order of magnitude. As a maximum of antiprotons had to be accumulated, the beam had large transverse dimensions and the AC provided a matching large transverse acceptance. However, this beam had to shrink very quickly, within 4.5 s, to a size fitting into the acceptance of the AA. This was achieved by using novel *plunging pick-ups and kicker electrodes*, which maximized the coupling to the beam. They had moving electrodes, which followed the shrinking of the beam as it was cooled [19]. Even this was not enough: the PUs, pre-amplifiers, terminating resistors and combiner boards had to operate at cryogenic temperatures — as low as 20 K — to minimize the thermal noise in the RF circuits, which substantially complicated the mechanical design. Figure 6.6 shows such a PU in its vacuum tank.

Two aluminium support structures (to the right and left) would move the many pickup loops (seen here as triangles) by 45 mm each towards the particle beam axis. The many horizontal channels (only their cross-sections are visible) were parts of the signal combiner for the multiple pickup loops. The upper and lower fixed aluminium support structures of 2.2 m length were holders of ferrite tiles absorbing undesirable microwave signals. The silver-plated undulated foils (adapting to the movement) were connections to fixed cold aluminium profiles. Similar flexible foils served as signal connections between the moving support structures and the vacuum feedthroughs. Fixed copper braids established the final thermal leads to the cryogenic sources. Six complete systems covering three adjacent bands in the 1 GHz to 3 GHz range were in operation in the AC. The two systems in each band were for horizontal and vertical cooling respectively; the sum signal of the two PUs served for longitudinal cooling.

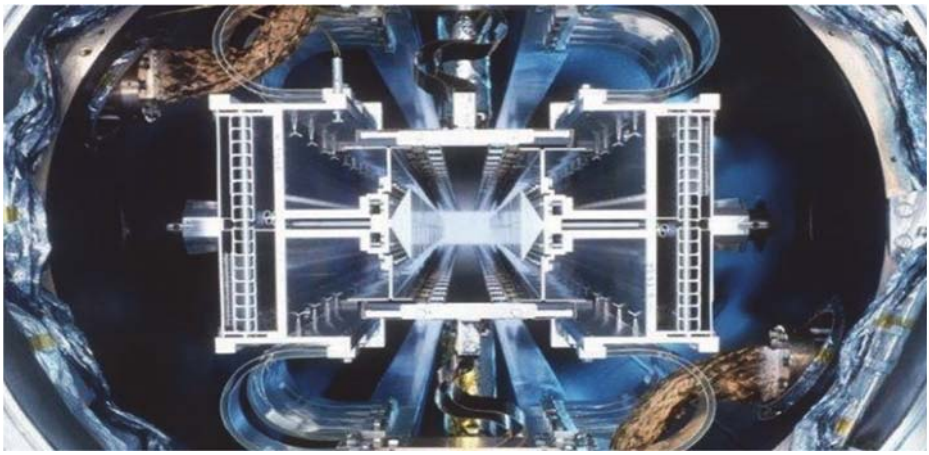

Fig. 6.6. Plunging PU in the AC, seen along the beam. The outer diameter of the vessel is 0.5 m.

The AC also required the development of 100 W *power amplifiers* for the bands 1–1.6, 1.6–2.4 and 2.4–3 GHz. These compact amplifiers were based on four power Field Effect Transistors (FET) per module and four modules per amplifier. Signal input splitting and output combination was performed with four-way elements absorbing electrical mismatches. This design was superior to the competing commercially available traveling wave tubes for several reasons: no high voltages, no cathode heating, better linearity, small phase change with amplitude and better life time [20]. The manufacture of the large series was entrusted to industry after a successful transfer of know-how.

6.3 Radio Frequency Quadrupole: Slowing Down Antimatter

Werner Pirkl

Many fundamental studies with antiprotons require extremely slow antiprotons, with velocities far below the kinetic energy of 5.31 MeV of the antiproton beam, extracted from the AD synchrotron [Highlight 6.7]. To this end a novel "Decelerator" was developed, a variant of the Radio Frequency Quadrupole (RFQ), which decelerated the antiprotons to 55 keV, followed by an integrated superimposed electrostatic energy correction to adjust the output energy between ~10 keV and 120 keV [21].

The RFQ is essentially a modified electric quadrupole consisting of two electrode pairs of opposite polarity, positioned at the diagonals of a square with the beam at the centre. This provides transverse focusing in one plane but causes defocusing at the orthogonal plane. Nevertheless, overall focusing can be achieved

by alternating static focusing and defocusing along the beam line. Alternation *in space* can be replaced by alternation *in time*. Feeding longitudinally continuous electrode pairs with properly chosen Radio Frequency (RF) provides also overall focusing due to the changes in polarity, as W. Paul, Nobel laureate 1989, had earlier demonstrated with linear "traps".

The decisive ingredient towards the RFQ was added in the seventies by "modulating" the radial distance of the electrode tips by opposite peaks and valleys in longitudinal direction [22]. This adds a longitudinal component to the transverse field pattern. Hence, the RFQ combines transverse focusing with longitudinal acceleration in a very compact geometry. It is therefore ideally suited for pre-accelerators up to the MeV range and supplanted quickly the traditional accelerator front-ends with their huge high-voltage Faraday cages.

The suitability of the RFQ for beam *de*celeration (RFQD) was quickly recognized [23, 24]. The basic electrode structure is the same as for the RFQ. A top view of four modulated electrodes is given in Fig. 6.7. Half of two electrodes is cut away for clarity. The distance between two electrode peaks, called a double cell, has to correspond to the time the particles travel during one RF cycle, being 4.94 ns in the case of the RFQD, determined by the operating frequency of 202.56 MHz.

As the velocity of the particles decreases gradually along the RFQD that distance decreases in proportion, here by a factor of about nine, from 157 mm at the input to 17.5 mm at the output. Contrary to accelerating RFQs it is no longer possible to use 30 to 50 double cells for "soft" beam capture and shaping as those are now on the high energy side, where their much longer cell length would lead to prohibitive overall length. Instead, bunching of the beam in a single step outside and upstream of the RFQD has to be used with less than perfect efficiency. Only about half of the beam falls in the acceptance of the RFQD.

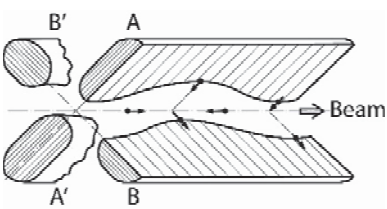

Fig. 6.7. The modulated electrodes of an RFQ; arrows show the electric field at a given moment.

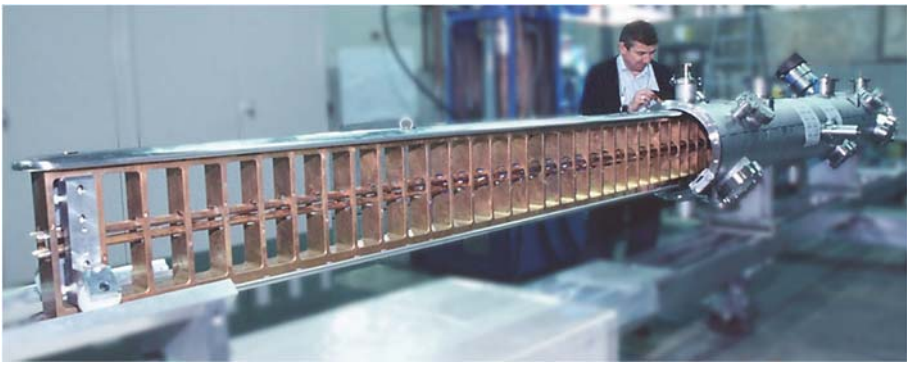

Fig. 6.8. The RFQD tank with the inner structure extracted for inspection.

The inner structure of the RFQD forms a "ladder" of length 3.4 m (Fig. 6.8). Continuous rails on top and bottom are connected by 35 rungs with the electrodes along the axis. The electrode pair A–A′ is connected to even-numbered rungs, pair B–B′ to the odd-numbered. All ladder parts are made of copper. The resulting 34 double-periodic cells are individually tuned to the operating frequency of 202.56 MHz. An RF amplifier chain (not shown) delivers the necessary RF power of more than 2 MW in 400 ns pulses at a repetition period around 300 s.

Figure 6.9 shows a cut through the RFQD in front of an even-numbered rung. Electrode pair A–A′ is firmly connected whereas pair B–B′ runs through an opening in the rung, at a distance of 10 mm to hold the RF operating voltage of 167 kV peak.

The ladder has to be mounted electrically "floating". It is held in place by two high-voltage (HV) insulators on the top and three on the bottom, where the central one acts also as a HV feedthrough for the energy-correcting voltage of +/− 65 kV DC, see Fig. 6.9. Curved HV shields on the vertical faces, made of stainless steel, prevent discharges. The inner face of the tank with 380 mm inner diameter is copper plated to reduce the RF losses.

Initial deceleration tests were carried out with a proton beam at the University of Aarhus, Denmark [25]. Current operation at CERN yields about one million decelerated antiprotons per shot. Compared to passive deceleration by degrader foils it provides a one to two orders of magnitude higher transmission together with improved beam quality which is close to the theoretical maximum for non-cooled deceleration.

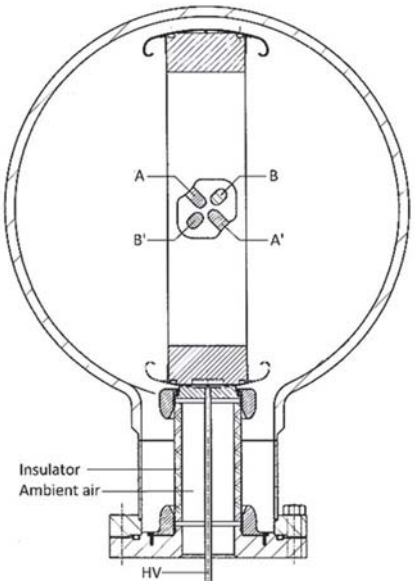

Fig. 6.9. Cross section of the RFQD.

6.4 The LEAR Ultra-Slow Beam Extraction: Trickling Antiprotons

Michel Chanel and Kurt Hübner

During the early discussions of the CERN proton-antiproton programme it was realized that antiprotons from the Antiproton Accumulator (AA) could be decelerated to lower energies providing pure, low-energy antiproton beams of unprecedented intensity for experiments [26]. This led to the construction next to the PS of a synchrotron ring of 78 m circumference, the Low-Energy Antiproton Ring (LEAR) [27] that was operating from 1983 to 1996. The beam, after injection from the PS at around 200 MeV (kinetic) energy, could be either accelerated up to 1270 MeV or decelerated to 5.3 MeV. At the chosen energy, the beam was left coasting either interacting with an internal target surrounded by a detector or extracted slowly and transferred to the experiments in the PS South Hall. The experimental programme embraced the study of p–$\bar{p}$ and $\bar{p}$–neutron interactions, of fundamental symmetries and the production of antihydrogen for matter–antimatter symmetry tests, and this called for new methods to manipulate beams.

Typically, a few 10^9 antiprotons, close to the minimum the PS could handle, were injected into LEAR. These particles were taken from the AA stack with an average consumption of 10^6 particles/s or about 10% of the AA accumulation rate and, hence, with little impact on the collider programme operated in parallel with

LEAR until 1991. Stochastic cooling and electron cooling of the beam was eventually used to control and to reduce the beam dimensions, particularly important at low energy. Electron cooling, invented in Novosibirsk [28] and tested in ICE, is based on the corrective action of "friction" experienced by particles deviating from the nominal momenta in a dense electron beam moving with the antiprotons over a small part of the circumference. It is particularly efficient at low energy.

In order to avoid saturating the particle detectors of the experiments, the users of the low-energy beams required an extraction rate, the spill rate, to be around 10^6 particles/s. Hence, for 10^9 antiprotons or more circulating the spill had to last about 10^3 s or longer, far beyond what had been achieved previously, e.g. typically 0.3 s in the PS. Compared to a one-time spill, the spill length of the beam arriving at the experiment had to be effectively stretched by a factor up to $3 \cdot 10^9$, implying that one would not skim off more than about one particle per turn from the circulating beam.

This problem was solved by stochastic slow extraction [29, 30] combined with a powerful feed-back system [31]. Slow-extraction is based on a mechanism which makes the amplitude of the horizontal particle oscillations grow on a time scale long compared to the revolution time. Once the amplitude is increased beyond a certain point the particles enter an electrostatic septum deflecting them into an external beam transfer channel guiding them to the experiments. The electrostatic septum provides the required electric field for this deflection at the edge of the aperture but shields the circulating beam from this field. The amplitude growth is generated by driving the particles into a resonance with a magnetic perturbation of proper azimuthal distribution introduced by design in the ring. Since there is a spread in the oscillation frequencies, the beam is gradually extracted. The oscillation frequency of the particles is expressed in terms of Q, the number of oscillations of the antiprotons per turn. The resonance occurs at a certain oscillation frequency Q_{res} outside the Q distribution of the beam. Since Q is a function of the revolution frequency, a modulation of the revolution frequency transforms into a modulation of Q. Hence, applying band-width limited white RF noise in a band at around a harmonic of the revolution frequency superimposes a noise spectrum on Q which can be positioned between Q_{res} and the Q distribution of the beam (Fig. 6.10); the particles diffuse in this noise band from the beam distribution to Q_{res}. The noise at a harmonic of the revolution frequency is generated by a kicker of the type used for longitudinal cooling which accelerates or decelerates the particles. The strength of the noise in Q is adjusted such that the particles diffuse towards the resonance at a speed determined by the required spill rate.

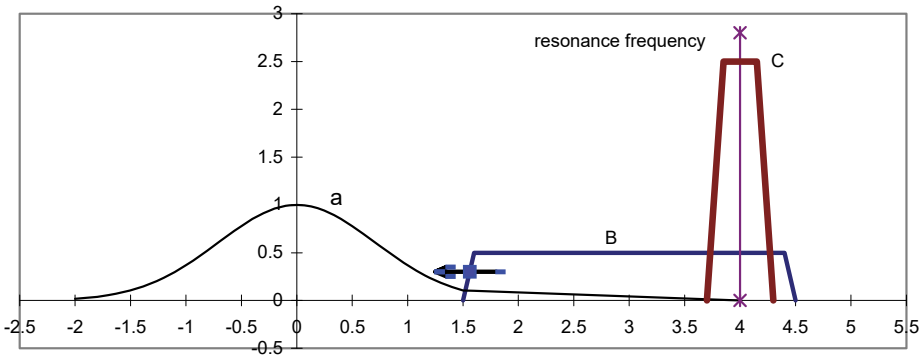

Fig. 6.10. Density distribution of antiprotons (a) and noise power spectra (B) and (C) versus $Q - Q_0$ where Q_0 refers to the centre of the beam distribution. Arbitrary units.

Particles slowly moving towards the resonance by diffusion in the noise band B are exposed to a much stronger noise C around the resonance. The low-frequency edge of band B is moved slowly into the stack eating into the distribution at the required rate. The band C increases strongly the diffusion rate once the particles are close to the resonance making the diffusion faster to reduce the adverse effects of the wobbling of the resonance which is brought about by the ripple in the powering of the magnets.

Two further steps were taken to smooth the spill in time. First, an air-core quadrupole was installed in the ring which was driven in antiphase of the mains ripple to strongly reduce the Q ripple and in turn the wobbling of the resonance. Secondly, the advance of the noise band into the stack was controlled by a sophisticated feed-back system, its input being an error signal derived from comparing the measured spill-rate at the experiment with the nominal rate.

Thanks to this set of measures spills lasting up to 14 hours eventually became routine, with spill-rates sufficiently low to satisfy the requirements of the experiments. Figure 6.11 shows an example of a spill lasting 10 hours where the beam was shared between two experiments by splitting the extracted beam.

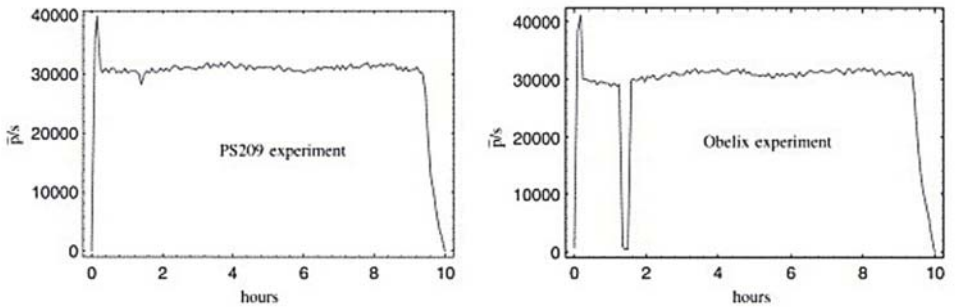

Fig. 6.11. Spill of antiprotons to two experiments. Each point on the curve is the number of particles recorded per s averaged over 10 s. The brief dip in the spill-rate of OBELIX is a pause for calibration.

6.5 The UA1 Tracker: An Electronic Bubble Chamber

Bernard Sadoulet

Physics goals and detector design philosophy

The priority for the UA experiments was the detection of the putative W and Z bosons of the Standard Model [Box 6.4] with emphasis on their "golden" signatures of their leptonic decay modes $W \rightarrow e\nu$ or $\mu\nu$ and $Z \rightarrow ee$ or $\mu\mu$, producing high transverse momentum charged leptons. Another major goal was the search for physics beyond the Standard Model, revealed by e.g. the simultaneous production of electrons and muons with specific charge configurations.

The accent was therefore put on the precise measurement of leptons, implying new performance requirements on the charged particle detector measuring the curvature of their tracks inside the magnetic field. The required excellent identification of the electrons would be obtained by comparing their momenta measured in the central tracker with their energies measured in the electromagnetic calorimeter. Muons would be identified as tracks penetrating through a metre of the iron return yoke of the magnet and by comparing the momentum measured in the central detector with that estimated from their deflection in the magnetized iron, obtained from the direction of the track emerging behind the yoke.

The measurement of high transverse momentum "jets" of particles was another design requirement of the UA1 detector. These jets could signal the emission of quarks or gluons, originating e.g. from the dominant quark–antiquark decay modes of the W and Z. Jets had been hinted at by experiments at the ISR (and later observed by AFS collaboration [Highlight 4.11], but at the ISR energy they were broad and difficult to identify. At the energy of the p–$\bar{p}$ collider, however, they were expected to be fairly easily detectable as a group of collimated particles.

Electromagnetic and hadronic calorimetry would measure their total energy, including the neutral particles (π^0's and neutrons).

The collaboration recognized rapidly that a detector was needed covering as much as possible of the solid angle around 90° from the beams. This is a prerequisite for the detection of the W or of any new physics based on "missing transverse energy", signalling the escape of a neutrino or possibly other neutral non-interacting particles such as supersymmetric particles [Box 7.2]. The design therefore aimed at achieving as close a "hermetic", i.e. 4π solid angle coverage, as possible, minimizing regions where particles could not be detected.

The geometry of the magnet was a major topic of discussion. The choice was between a solenoid coaxial with the beams or a dipole with its field perpendicular to them. While considerations of symmetry favoured a solenoid, a dipole was finally chosen. This was motivated in large part by the requirement of a detector with a fairly large aspect ratio (6 m long with a diameter of 2.5 m), in order to match the topology of the final states produced in the collisions. A solenoid would have to be instrumented with a self-supporting drift chamber with 6 m long wires, for which the technology was not available, and the CERN engineering team came forward with a very elegant solution for a tracking detector optimized for the dipole [Box 4.4]. To meet the short construction time a conventional warm magnet was adopted with a 0.7 T field and a magnetic volume of 80 m^3.

The UA1 tracker

With the spectrometer magnet chosen, the collaboration converged rapidly on the technology of the central detector. This instrument had to offer very good spatial resolution, high efficiency for reconstructing tracks in events of very high particle multiplicities and a bubble-chamber like clarity of the track pattern to clearly expose the precious leptons. The "Time Projection Chamber", invented in 1974 [32], shows this kind of performance and this concept was adapted to the UA1 magnet geometry. Instead of measuring the track curvature in projection, the measurement of the drift time was used due to its intrinsic precision; this led to having the sense wires parallel to the magnetic field. The design goal materialized in a drift chamber system with 6000 sense wires [Box 4.5]. The novel electronic read out could register several independent hits on a drift wire per collision, simultaneously digitizing the drift time and the charge information, which allowed a pictorial track reconstruction in three dimensions. At the time, this tracker (Fig. 6.12) was at the frontier of drift chamber development [Highlight 4.8].

Detecting invisible particles **Box 6.3**

Particles properties are revealed in particle detectors, devices in which the particle "interacts" and leaves a telltale signal [Box 3.2]. No single detector can measure all their properties and several specialized ones are combined in an experiment. Through electromagnetic (e-m) interaction, charged particles ionize or excite a specially chosen material in the detector. It may be a gas [Highlight 4.8], a liquid [Highlight 5.6] or a solid [Highlight 5.9]. The level of ionization or excitation depends characteristically on the particle velocity v [Box 5.2]. A variety of detectors have been developed to measure position, velocity and energy of the particles.

Tracking detectors measure the charged particle position or trajectory. They have one important and distinct feature: a very gentle interaction, hardly influencing the properties of the particle, suffices to produce a useful signal.

When these detectors are immersed in a magnetic field B, the radius of curvature ρ of the charged track, proportional to p/qB (where q is the charge), gives its *momentum* p. The figure of merit of such a "spectrometer" is its accuracy, expressed as $\Delta p/p, \approx p\ \sigma/\ B\ L^2$, where σ is the precision of the position measurement and L the distance over which the particle track is analysed. This explains the quest for improved σ and higher B, and the increasing size (L) of the spectrometers to measure ever increasing p [Highlight 8.12].

Other instruments measure the *energy* E. Interacting via e-m and/or strong interaction the particle develops a *cascade ("shower")* of particles absorbed in a massive detector. Nearly all E of the incident particle is finally transferred to excitation of the absorber molecules, increasing its temperature, whence the name "*calorimeter*". The absorber is usually instrumented with detectors sensitive to the cascade of particles [Highlight 4.10], but can also be sensitive in its full volume [Highlight 7.9]. The number of cascade particles being proportional to E, the statistical accuracy of the E measurement is $\approx 1/\ E^{1/2}$, a bonus for high E. Calorimeters work for both charged and neutral particles.

To *identify a particle* via its mass, one needs p and its velocity v. Besides time of flight measurement for slow particles [Highlight 8.9], one uses also the v dependence of e-m processes: ionization, Cherenkov or transition radiation [Highlights 4.9, 7.8]. Charm or beauty particles live of the order of 10^{-12} s. Being produced with v close to the speed of light, the relativistic time dilation lets them fly of the order of 1 mm before decaying, a decay pattern accessible to Pixel detectors [Highlight 8.6]. Assembling such specialized detectors leads to the typical onion-like sequence at colliders. "Fixed target" experiments (such as COMPASS, Chapter 5) have a quite different structure.

These detectors, first developed for particle physics, are now frequently found in medical diagnostic and imaging techniques [Highlights 10.3, 10.4].

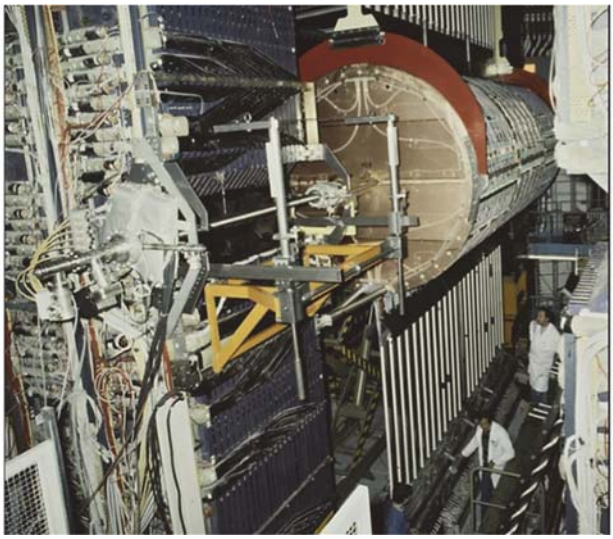

Fig. 6.12. Partial view of UA1. The detectors surrounding the long, cylindrical central tracker are retracted to provide access to the Tracker. The thin beam pipe traverses the centre of the tracker.

The mechanical design was very innovative. As a self-supporting cylinder, made of six independent half-cylinder chambers, each with a length of 2 m and a diameter of 2.2 m (Fig. 6.13a), it provided close to 4π coverage of the collision products and achieved the bubble chamber-like "view" of the events (Fig. 6.14). One striking feature of the system was the cylindrical shell of the chambers supporting the wires, made with a pre-stressed honeycomb structure, sandwiched between glass fibre-epoxy layers. The amount of applied pre-stress was calculated to precisely balance the tension applied to the wires.

The 6000 sense wires (10 mm spacing, up to 2.2 m length) and the 17 000 field-shaping wires were parallel to the magnetic field. They were organized in horizontal planes in the four forward modules, and in vertical planes in the two central ones. This arrangement is a consequence of the horizontal magnetic field. With this orientation of the wire planes approximately the same number of measurements along the tracks over the detector volume was obtained, given the expected topology of the interactions and the dipole magnetic field. A typical drift cell is shown in Fig. 6.13b. The electrostatic forces were controlled with an intermediate field plane at voltage V_c, while V_f controlled the gas amplification. The position of the sense wires in a plane was known within 50 microns, the coordinate of a "typical" plane to about 200 microns, a tribute to the engineering quality of the supporting structure.

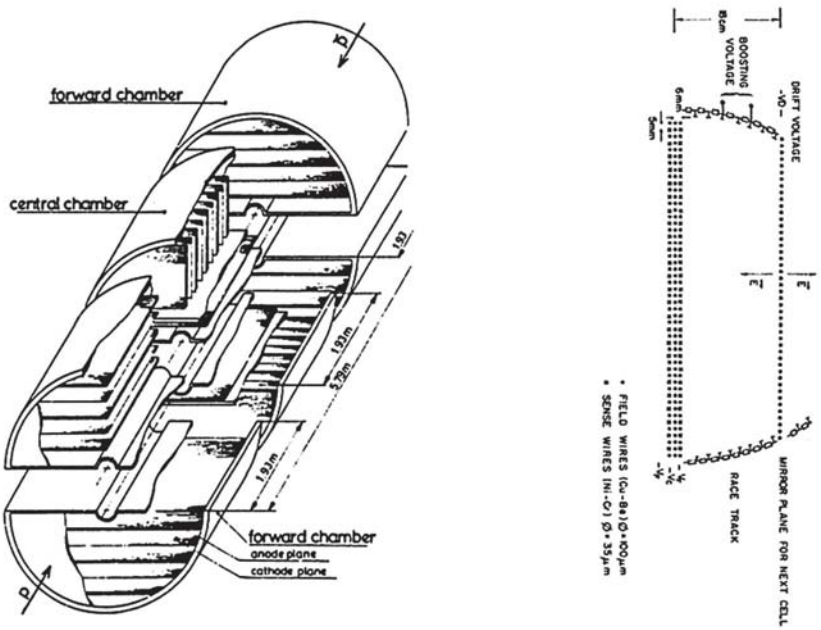

Fig. 6.13. Left: exploded view of the six half-cylinders constituting the central tracker; right: cross-section through a half-cylinder, showing the arrangement of signal wires and wire electrodes shaping the drift field and the signal amplification region.

The longest drift distance was 18 cm, such that at a 1.5 kV/cm drift field the drift time was less than the interval between bunches (3.8 μs). This drift length also limited the distortion of the electric field by space charge from backgrounds from the machine. The state-of-the-art signal processing used 6-bit "Flash Analogue-to-Digital Converters (FADCs), two per sense wire, digitizing the induced signal charge. The sense wire had kΩ level resistance; the ratio of the charges recorded at each end gave a measure of the longitudinal position of the charge along the wire to about 2% of the wire length. The drift time was measured with Time-to- Digital Converters (TDCs) with 4 ns accuracy. The digital outputs of TDCs and FADCs were stored in a buffer memory, recording the event history of the preceding 4 μs. The data volume (1.6 MB) was impressive at the time and had to be synchronously reduced by processors.

The analogue signal processing electronics required careful calibration. The linearity was calibrated by injecting a precisely known and variable charge into the preamplifiers. For each drift cell, the relevant voltages and currents were precisely measured and monitored. An alarm system provided fast indications of any malfunctioning.

To achieve the intrinsic performance of the tracker a number of parameters had to be measured and controlled, such as temperature, gas mixture variations and distortions of the electric fields. Two independent methods were used. Artificial straight tracks were generated with precisely positioned ionizing X-ray and laser beams. Secondly, the built-in "auto-calibration" of the detector was used, made possible by the special drift cell structure: as two adjacent drift spaces had opposite E-fields, tracks traversing them had to "line up" in a correctly calibrated detector. These efforts paid off. The globally achieved resolution of the drift distance was a most remarkable 290 microns for the reconstructed tracks.

Figure 6.14 shows an historical event, the first W decay recorded in the UA1 experiment. With its combination of optimal detection geometry, matching well the expected interesting collision topologies, an advanced technology for the support structures, innovations in electronics, calibration and read-out, this tracker was at the cutting edge of technology and the first true "electronic bubble chamber". Its quality and reliability were a key to the Nobel Prize-winning success of UA1.

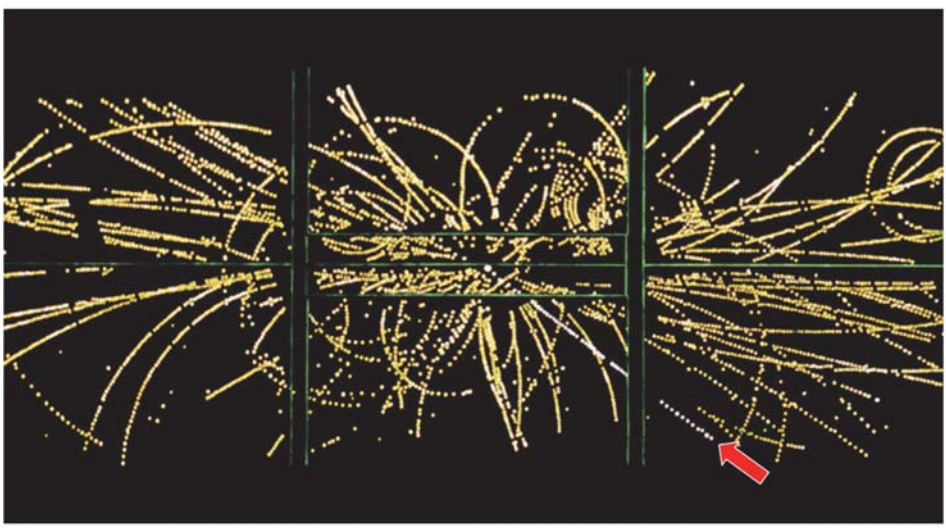

Fig. 6.14. The first observed W-decay, as recorded in the central tracker.

The Standard Model (SM) **Box 6.4**

The SM is a remarkably successful theoretical description of the elementary particles and their interactions, from which our visible world is built. It ignores gravity, described by the General Theory of Relativity. Figure 1.2 shows the SM constituents (fermions of spin 1/2). The carriers of the 3 types of forces between fermions, bosons of spin 1, are shown in Fig. 1.3. To these elementary objects, one must add the spin 0 Higgs boson.

The SM describes mathematically the particles as field quanta. These exist not only in space-time, but also "live" in abstract, so-called *internal spaces* (Fig. 1.2). E.g., a quark lives in the 3-D space of *colour*, in which it can be thought of as a vector. The subscripts L (Left) and R (Right) refer to their handedness H [Box 2.2] and point at a basic feature of the SM that the behaviour depends on H: in the *weak isospin* (WI) *space,* LH ones live in couples, RH ones as singles. In the SM the W couples only to LH fermions.

In such spaces, one can think of performing "rotations": for instance, a rotation in colour space changes a blue quark into a red quark. Or, in the WI space, an e^- rotates into a neutrino, or a strange quark into a charm quark. The SM gives the processes: emission of a gluon in the former case, of a W boson in the latter. There is thus a unique mode of interaction between fermions, whatever the force: the exchange between them of the relevant boson, as suggested by the diagrams of Fig. 1.3.

The SM provides the mathematical framework describing these rotations. But it does much more: its guiding principle posits the freedom to perform any arbitrary such rotation *locally,* i.e. in any point of space-time, without changing the physics, which cannot depend on an arbitrary choice of local coordinates. The equations of the SM must thus be invariant (symmetrical) under the relevant rotation. This symmetry requirement is a great help in defining the actual mathematical formulation. Such a rotation of the field configuration is called a "gauge" transformation (GT). The lack of change (invariance) of measurable quantities under a GT is called *gauge invariance*.

In quantum electrodynamics, QED [Box 2.3], describing e.g. the e^- and γ, the GT changes the phase of the e^- wave function, through γ emission by the e^-. The γ feels the e^- electric charge but does not carry it. Being neutral it does not self-interact (SI).

An important success of the SM is a unified description of QED and the weak interaction, the Electroweak Interaction. Its "abstract" bosons W^0, B^0 (not shown in Fig. 1.3) "mix" to give the physical γ and Z^0, through the mixing angle θ_W [Box 7.1]. The initial unified formulation (in 1961) only worked however for massless particles, and could not explain fully our perception of reality. The BEH mechanism [Box 8.2] completed the picture, enabling the SM to much better describe the visible world.

In the weak and QCD sectors, W/Z and gluons feel and carry the weak and colour charge, respectively, and *self-interact*. Gluon SI is responsible for the specific properties of the strong interaction [Box 4.2].

6.6 A Novel Particle Detector for UA2: The Power of Silicon

Claus Gößling and Pierre Jarron

In 1983 — the UA1 and UA2 collaborations had just discovered the W and Z bosons — the UA2 collaboration decided to upgrade its tracking detector by replacing part of the existing detector with a silicon detector [33]. It represented a major step forward in silicon detector technology, replacing the conventional strip-geometry of the detector elements [Highlight 5.9] with a novel checkerboard or "pad" configuration, providing improved track reconstruction. This detector worked very well. It encouraged the collaboration in 1986 [34] to push this concept further and to develop a second Silicon Pad Detector (SPD) with finer pad segmentation to be placed directly around the collision interaction beam pipe.

The layout of the new inner SPD matched the detector geometry of the outer silicon detector in order to optimize track reconstruction. The detector was built as a cylinder surrounding closely the beam pipe in the available radial thickness of 9 mm, with almost no dead space. The size of the pads was 17.3×33.5 mm^2; they provided 3072 channels. It was the first incarnation of a silicon tracker with a detector geometry adapted to a collider experiment, an ancestor of the present silicon vertex detectors.

The project presented several challenges: the barrel detector had to fit into the available radial space of less than 1 cm, including silicon sensors, electronics and associated circuit boards. Miniaturization of the detector was mandatory and was achieved with at that time two brand new technologies, the silicon sensor [35] and an Application Specific Integrated Circuit (ASIC), representing totally new approaches in particle physics experimentation. At that time tracking technology was based on gaseous detectors (MWPC) [Highlight 4.8] and discrete electronics comprising miniaturized components with hybrid electronic technology.

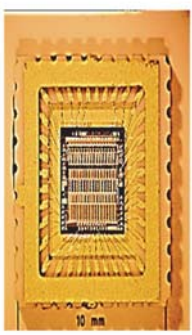

Fig. 6.15. ASIC AMPLEX, a 16 channel readout system developed for the Inner Silicon Pad Detector.

Developing the readout electronic system scaled to the miniaturized dimensions of the SPD represented probably the biggest challenge. Existing electronics was too bulky — incompatible with the required thickness and the channel density of the UA2 Silicon Pad Detector. It required the development of a novel ASIC tailored to the UA2 silicon sensors and experimental requirements. Figure 6.15 shows the device mounted in a 10 × 10 mm^2 package. All 16 electronics channels, providing the readout of 16 pads, were contained in a silicon die of 4 × 4 mm^2.

The ASIC, called AMPLEX [36], was fabricated in a 3 μm gate length CMOS technology. Stringent requirements were placed on the electronic noise, because a relatively tiny charge of about 24 000 electrons (4 fC) is produced by a minimum ionizing particle in 300 μm thick silicon. The typical noise figure obtained with the AMPLEX input amplifier stage was the equivalent of 1200 e^- r.m.s. resulting in an excellent signal-to-noise ratio of 20. Power consumption per channel was 1.5 mW.

The second feature of the AMPLEX circuit was the readout technique. The CERN proton–antiproton collider had a machine cycle of 3.8 μs. Therefore, the signal had to be available within 2–3 μs for a possible "readout decision" within the machine cycle prior to the serialized readout of the analogue signals of all channels. An appropriate signal shaping circuit was implemented, a proven electronic design for nuclear instrumentation, followed by a sample-hold circuit.

One further critical step in the construction was the assembly of the silicon detectors and electronics. A stave-like long multilayer-board, 3.5 mm thick, carried on the outer side all the AMPLEX-ASICs (plus a few capacitors) and on

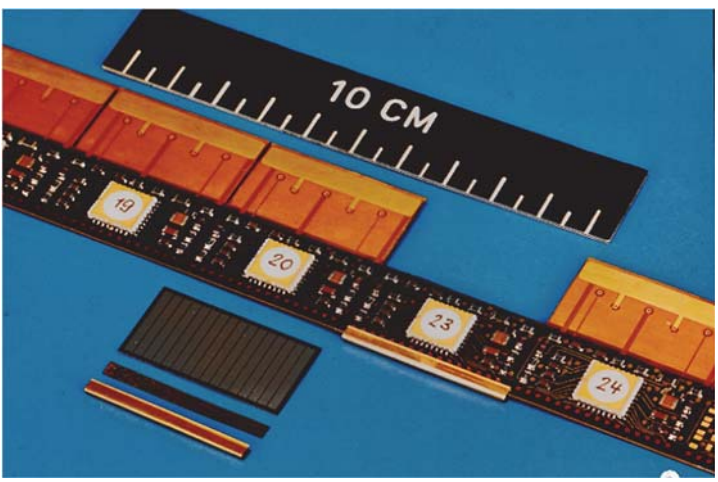

Fig. 6.16. Assembly of the silicon pad sensor and AMPLEX ASIC's on the stave.

the inner side the silicon sensors. The electric contact from the sensor to the multilayer-board was established by a strip of vertically conductive rubber under mechanical pressure of an elastic clip. A similar approach has been later used for the construction of the silicon tracker and vertex of ATLAS and CMS [Highlight 8.6].

The assembled and tested detector boards were positioned on a carbon fibre support, prior to insertion into the UA2 detector (Fig. 6.17). The insertion of the detector was assumed to be a trivial task, until it was realized that the detector diameter was 0.3 mm bigger than the available space of 9 mm. As always, the devil is in the details. The problem was solved by replacing certain capacitors which were out of specification and the Inner UA2 Silicon Pad Detector was successfully installed.

Both UA2 Silicon Pad Detectors performed very reliably during the data-taking from 1987 up to the end of operation at the p–$\bar{p}$ collider in 1991. The unambiguous two-dimensional tracking information was instrumental for the pattern recognition of the many secondary tracks produced in these p–$\bar{p}$ collisions. The AMPLEX chip was the first complex readout chip operating inside the sensitive volume of an inner detector and in the direct vicinity of the interaction point.

Fig. 6.17. Insertion of the inner silicon pad detector into the UA2 detector.

6.7 Antimatter's Disappearing Act

Michael Doser

Many attempts have been made to explain the apparent complete absence of antimatter in the Universe, which runs counter to the expectation that right after the Big Bang, both matter and antimatter should have been present in equal amounts. Although some of the proposed explanations have been experimentally investigated and identified, they do not suffice. Further mechanisms remain to be discovered. Searching for minute differences between the properties of particles and their antiparticles lies at the heart of many of these attempts, and still holds out the best chance at sniffing out the culprit. The challenges are daunting: on one hand, fundamental symmetries and conservation laws set severe limits on any possible differences between particles and antiparticles, and finding any such differences would trigger a scientific revolution; on the other hand, carrying out precision experiments on antimatter systems requires developing or adapting techniques that go far beyond the state of the art. Progress in this field has thus been slow, if relentless, and is closely tied to invention and implementation of new technologies.

Most amenable to being precisely studied are individual stable antiparticles, or systems composed of them: antiprotons, positrons or antihydrogen atoms. While it is relatively straightforward to obtain positrons (from the radioactive decay of radioisotopes such as ^{22}Na), or to form antiprotons (which requires particle accelerators, and was first done in 1955 at the BEVALAC at LBL, and subsequently carried out at CERN on a quasi-industrial scale from 1980 onwards), precision studies require antiparticles at energies that lie many orders of magnitude below what can be achieved at accelerators, μeV instead of GeV. Furthermore, with minute numbers of antiparticles to work with, detection of their signals will always be daunting: either their detection will be non-destructive, in which case electronic noise represents the largest background, or their detection will be destructive, in which case background from cosmic rays (which can occasionally mimic annihilation topologies) represents the largest challenge. But before tackling these hurdles, the first crucial technology that needed to be developed was trapping of antiparticles.

Antiprotons are produced at CERN by colliding 24 GeV protons from the Proton Synchrotron with a fixed target (made of copper); the tiny fraction of antiprotons produced in these collisions (one antiproton–proton pair per million collisions) are filtered out by mass and charge. They are subsequently decelerated from their initial energy of several GeV down to 5.3 MeV at CERN's Antiproton Decelerator (AD). Trapping these requires a further reduction in energy. The TRAP collaboration conceived and successfully implemented the first such scheme in 1986 [37]: like all

charged particles, antiprotons lose energy by interacting with the electrons of the atoms of any material that they traverse. Furthermore, charged particles with energies below a keV can be easily manipulated electromagnetically (in vacuum) within so-called Penning traps (stacks of ring-shaped electrodes held at different electric potentials, and situated inside a strong magnetic field). The TRAP collaboration thus placed a thin foil (whose thickness was chosen to maximize the tiny fraction of antiprotons coming out with energies below a few keV) upstream of a Penning trap whose furthest electrode was held at several kV. Before the "slow" reflected antiprotons (whose velocity is of the order of 1000 km/s, or 1 m/μs) could return, they rapidly switched the first ring (immediately after the foil) from ground potential to the same high voltage. The energy of these now trapped antiprotons can then be further reduced (via "electron cooling") from keV down to meV, where their properties are studied precisely by the ATRAP and BASE experiments [38]. It is these cold antiprotons that, combined with cold positrons, can form antihydrogen atoms, as demonstrated for the first time in 2002.

The first method for producing cold antihydrogen was developed by the ATHENA and ATRAP collaborations and subsequently improved by the ALPHA collaboration, all working at CERN (Fig. 6.18). This method consists of setting up a specific configuration of electric fields inside a Penning trap, in order to create an overlap between a cloud of cold antiprotons and a cloud of positrons. Formation of an antihydrogen atom requires three partners: an antiproton, a positron, and an additional positron which carries away the binding energy of the newly formed antiatom. Demonstrating that this process is taking place means detecting these antihydrogen atoms. Once formed, they are neutral, and are free to drift through the electric and magnetic fields of the Penning trap. The scheme developed by ATHENA relies on imaging the annihilation products that appear when the antihydrogen atoms reach the inner surface of the Penning trap rings. A multilayer silicon microstrip detector, coupled with a CsI-based photon detector, all operating at cryogenic temperatures, allowed reconstructing the trajectories of the charged particles produced in the annihilation of the antiprotons (and thus the position of the annihilation vertex), as well as detecting the direction and energy of the photons produced in the annihilation of the positrons (Fig. 6.18). Such imaging detectors were crucial not only in demonstrating the production of antihydrogen [39], but also in elucidating the complex plasma dynamics taking place in its formation, and enabled the ALPHA collaboration to take the crucial next step, that of trapping the coldest formed atoms.

In order to study the formed antihydrogen atoms, they must either be shaped into a beam (as done in the ASACUSA experiment) or trapped. Although electrically neutral, antihydrogen atoms can be trapped in a magnetic multipole

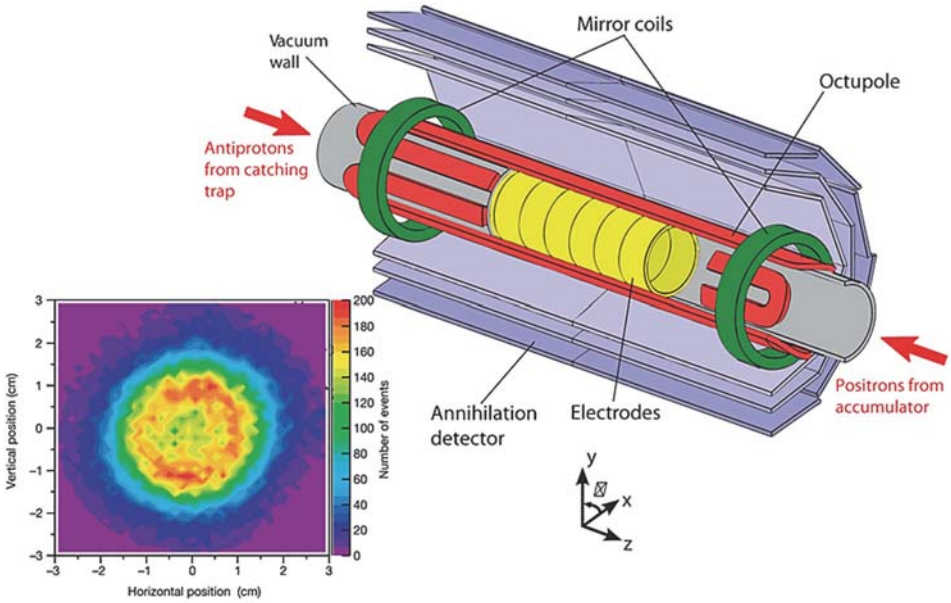

Fig. 6.18. Left: Distribution of reconstructed antiproton annihilation vertices in the ATHENA experiment, reflecting the formation and subsequent annihilation (on the inner Penning trap surfaces) of antihydrogen atoms. The colour code (violet to red) corresponds to number of detected annihilations [39]. Right: A schematic, cut-away diagram of the antihydrogen production and trapping region of the ALPHA apparatus, showing the relative positions of the electrodes, the minimum-B trap octupole (red) and axial pinch (green) magnets and the 3-layer silicon microstrip antihydrogen annihilation detector [41].

trap (with a field minimum at its centre) through the interaction between the antihydrogen atoms' internal energy states and the magnetic field. Technical limitations on the magnets however entail that only the coldest atoms, with a temperature of less than 0.5 K, can be trapped this way, while the bulk of the formed atoms have temperatures far in excess of this value.

Detecting the tiny fraction of (possibly) trapped atoms required another technical breakthrough: rapid switching of magnetic multipole traps. To prove that they had formed and trapped antihydrogen atoms, the ALPHA collaboration opened their magnetic multipole trap, allowing antihydrogen to escape and annihilate. A major confounding background signal comes from cosmic rays interacting in their apparatus, which occasionally mimic signals associated with antiproton annihilations. Reducing this background is thus of tantamount importance, and one way to do this is to ramp down their multipole trap more rapidly than the 10 seconds usually required to reduce the current of the

superconducting trap. The ALPHA design [39] relies on a unique technique developed at BNL [40] that provides great freedom in defining the winding patterns of the magnet, as well as great mechanical strength, and that allows a current decay time of 9 ms. Using these technologies, the ALPHA experiment could establish trapping of single antihydrogen atoms in 2010 [41]. Other exotic atoms containing antiprotons are also possible: ASACUSA uses precision lasers to study antiprotonic helium, in which an electron in helium is replaced by an antiproton.

The field of antihydrogen physics will continue to place great demands on new technologies, as the experiments move deeper into the field of atomic physics. The current generation of experiments is working towards first precise comparative studies of antihydrogen and hydrogen. The next few years should see optical and microwave spectroscopy of antihydrogen, as well as first tests of the gravitational behaviour of antihydrogen atoms by the AEgIS, GBAR and ALPHA-g experiments. Reaching and going beyond these initial steps, into the domain of high precision studies, will however require cooling of trapped antihydrogen atoms to their recoil limit of ~ 2 mK, development of new cooling techniques to enter the realm of sub-mK temperatures, and enhancement of the formation rates of ultra-cold antihydrogen atoms by orders of magnitude. An increasingly large and interdisciplinary community is focused on developing the necessary technologies that will allow the experimental sensitivities to gradually reach the range where fundamental discoveries could become possible.

References

1. H. Koziol and D. Möhl, The CERN antiproton collider programme: accelerators and accumulation rings, *Physics Reports* **403-404**, 91 (2004).
2. S. van der Meer, Stochastic damping of betatron oscillations in the ISR, CERN-ISR-PO/72-31 (1972), https://cds.cern.ch/record/312939/files/197200067.pdf.
3. P. Bramham, G. Carron, H.G. Hereward, K. Hübner, W. Schnell and L. Thorndahl, Stochastic cooling of a stored beam, *Nucl. Instr. & Meth.* **125**, 201(1975).
4. C. Rubbia, P. McIntyre and D. Cline, Producing massive intermediate vector bosons with existing accelerators, *Proc. International Neutrino Conference*, Aachen, Germany (June 1976) pp. 683–687.
5. G. Carron *et al*., Stochastic cooling tests in ICE, *Phys. Lett. B* 77, 353-354 (1978).
6. V. Chohan *et a*l., The CERN Antiproton Accumulator Complex (AAC): current status and operation for the nineties, in *Proc. 15th International Conference on High-energy Accelerators*, Hamburg, Germany (July 1992) pp. 106-108.
7. S. van der Meer, Stochastic cooling in the CERN antiproton accumulator, *IEEE Trans. Nucl. Sci*. **28**, 1994-1998 (1981).

8. E. Jones, ACOL, CERN's Upgrade of the antiproton accelerator complex, *Proc. 6th Topical Workshop on Proton-Antiproton Collider Physics*, Aachen, Germany (June 1986) pp. 691-704.
9. H. Koziol and D. Möhl, The CERN low-energy antiproton programme: the synchrotrons, *Physics Reports* **403-404**, 271-280 (2004).
10. C. Rubbia, The discovery of the W and Z bosons, *Phys. Rep.* **239**, 241 (1994);
    P. Darriulat, History of original ideas and basic discoveries in particle physics, *NATO ASI Series B. Phys.* **352**, 757 (1996), and *Eur. Phys. J. C* **34**, 33 (2004).
11. D. Denegri, When CERN saw the end of the alphabet, *CERN Courier*, April 30, 2003;
    L. Di Lella, *Proc. XXXII Int. Meet. on Fund. Phys.*, Alicante, ed. CIEMAT, Madrid (2004) 291.
12. M. Barranco Luque *et al.*, The construction of the central detector for an experiment at the CERN anti-p p collider – UA1, *Nucl. Instr. & Meth.* **176**, 175 (1980);
    M. Calvetti *et al.*, *Nucl. Instr. & Meth.* **176**, 255 (1980);
    K. Eggert *et al.*, *Nucl. Instr. & Meth.* **176**, 217 (1980);
    A. Astbury, *Physica Scripta* 23, 397 (1981).
13. A.G. Clark *et al.*, *Proc. Int. Conf. on Inst. for Coll. Beam Phys.*, SLAC-250 (1982); p. 67 in *2nd Int. Conf. on Phys. in Colliders*, Stockholm (Plenum, New York, 1983);
    B. Mansoulié, p. 609 in *Proc. 3rd Moriond Workshop on $\bar{p}p$ Physics*, (Editions Frontières, 1983);
    A. Beer *et al.*, The central calorimeter of the UA2 experiment at the CERN anti-p p collider, *Nucl. Instr. & Meth.* **224**, 360 (1984);
    K. Borer *et al.*, *Nucl. Instr. & Meth. A* **257** (3), 591 (1987);
    R.E. Ansorge *et al.*, *Nucl. Instr. & Meth. A* **273** (2), 826 (1988).
14. J.G. Rushbrooke *et al.*, *Physica Scripta* 23, 642-648 (1981);
    G.J. Alner *et al.*, UA5: A general study of proton-antiproton physics at $\sqrt{s}$ = 546 GeV, *Physics Reports* **154**, 247-383 (1987).
15. M. Amoretti *et al.,* Production and detection of cold antihydrogen atoms, *Nature* **419**, 456-459 (2002);
    G. Gabrielse *et al.,* Background-free observation of Cold Antihydrogen with field-ionization analysis of its states, *Phys. Rev. Lett.* **89**, 213401 1-4 (2002).
16. S. van der Meer, Stochastic Cooling and the Accumulation of Antiprotons, *Rev. Mod. Phys.* **57**, 689-697 (1985).
17. G. Carron and L. Thorndahl, Stochastic Cooling by filter techniques, *CERN Internal Report* CERN-ISR-RF-78-12, (1978), http://cds.cern/record/119952/files/19704143.pdf.
18. L. Faltin, Slot-type pick-up and kicker for stochastic beam cooling, *Nucl. Inst. & Meth.* **148 (**3), 449-455 (1978).
19. B. Autin, G. Carron, F. Caspers, S. Milner, L. Thorndahl and S. van der Meer, ACOL stochastic cooling systems, *Proc. Part. Accel. Conf. (PAC 1987)*, Washington, USA (1987) pp. 1547-1551.
20. G. Carron, F. Caspers and L. Thorndahl (eds.), *Development of Power Amplifier Modules for the ACOL Stochastic Cooling Systems*, CERN-1985-001, (CERN, Geneva, 1985). http://dx.doi.org/10.5170/CERN-1985-001.
21. Y. Bylinsky, A.M. Lombardi and W. Pirkl. RFQD: a decelerating RFQ for the CERN antiproton facility. *Proc. 20th Int. Linac Conf.*, Monterey, USA (Aug. 2000) pp. 554-556. http://accelconf.web.cern.ch/AccelConf/l00/papers/TUD05.pdf.
22. I.M. Kapchinskij and V.A. Teplyakov. Ion linear accelerator with spatially homogeneous strong focusing. *Prib. i. Tekhn. Eksp. (Instr. and Exp. Techn.)* **2**, 19-22 (1970).

23. C. Biscari and F. Iazzourene, Post-deceleration of the LEAR beam by a radiofrequency quadrupole. *Proc. 3rd LEAR Workshop,* Tignes, France, (Jan., 1985) pp. 115-120, http://cds.cern.ch/record/159830/files/cer-000071161.pdf.
24. J. Bosser *et al.* (ed. W. Pirkl). Feasibility study of a decelerating Radio Frequency Quadrupole system for the Antiproton Decelerator AD, *CERN internal report CERN/PS/HP Note* 97-36, (1998), http://cds.cern.record/558230/files/open-2002-040.pdf.
25. A.M. Lombardi, W. Pirkl and Y. Bylinsky. First operating experience with the CERN decelerating RFQ for antiprotons. *Proc. 2001 Part. Accel. Conf.*, Chicago, USA (2001) pp. 585-587, http://accelconf.web.cern.ch/accelconf/p01/PAPERS/ROPA009.pdf.
26. K. Kilian, U. Gastaldi and D. Möhl, Deceleration of antiprotons for physics experiments with low-energy antiprotons, *Proc. 10th Int. Conf. on High-Energy Accelerators*, Protvino, USSR, (1977) pp. 179-184.
27. https://home.**cern**/about/accelerators/low-energy-antiproton-ring.
28. G.I. Budker, Status report of the work on storage rings at Novosibirsk. *Proc. Symp. Int. sur les Anneaux de Collisions à Electrons et Positrons*, p.II-1-1, Saclay, France (1966).
29. S. van der Meer, Stochastic Extraction- A low ripple version of resonant extraction, *CERN Int. Report CERN/PS/AA* 78-6 (1978), http://cds.cern/record/118881/files/cer-000029365.pdf.
30. R. Cappi, R. Giannini and W. Hardt, Ultra-slow extraction – Status report, *CERN int. report CERN-PS-LEA-82-3*, presented at LEAR Workshop, Erice, Italy, (June 1982). http://cds.cern/record/1414413/files/CERN-PS-LEA-82-3.pdf.
31. S. Jacobsen, G. Molinari and H. Mulder, A feed-back system to control the flux during ultra-slow extraction at LEAR, *Proc. 6th European Particle Accelerator Conference (EPAC96)*, Sitges, Spain (June 1996) pp. 1845-1847.
32. D.R. Nygren, Proposal to Investigate the Feasibility of a Novel Concept in Particle Detection, *LBL internal report*, February 1974;
J.N. Marx and D.R. Nygren, *Physics Today* **31**(10), 46 (1978).
33. K. Borer *et al*., Construction and performance of a 1 m^2 silicon detector in UA2, *Nucl. Instr. & Meth. A*, **257**, 591–593 (1987).
34. K. Borer *et al*., The implementation and performance of a 1 m^2 silicon hodoscope array in UA2 and proposed construction of a second array, *Nucl. Instr. & Meth. A* **273**, 605-610 (1988).
35. E.H.M. Heijne and P. Jarron, The impact of microelectronics on particle detection, *Nucl. Instr. & Meth. A*, **226**, 12-15, (1984).
36. E. Beuville *et al.*, Amplex, a low-noise, low-power analog CMOS signal processor for multi-element silicon particle detectors, *Nucl. Instr. & Meth. A* **288**, 157 (1990).
37. G. Gabrielse *et al*., First capture of antiprotons in a Penning trap: A kiloelectronvolt source, *Phys. Rev. Lett.* **57**, 2504 (1986).
38. G. Gabrielse *et al.*, Cooling and slowing of trapped antiprotons below 100 meV, *Phys. Rev. Lett.* **63**, 360 (1989).
39. W. Betsche *et al.* (ALPHA collaboration), A magnetic trap for antihydrogen confinement, *Nucl. Instr. & Meth. A* **566**, 746 (2006).
40. http://www.bnl.gov/magnets/BEPCII/BEPCII.asp.
41. G.B. Andresen *et al*., (ALPHA collaboration), Trapped antihydrogen, *Nature* **468**, 673 (2010).